

Optical and radio measurements of a 630-nm airglow enhancement over Japan on 9 September 1999

Y. Otsuka, T. Kadota,¹ K. Shiokawa, and T. Ogawa

Solar-Terrestrial Environment Laboratory, Nagoya University, Aichi, Japan

S. Kawamura and S. Fukao

Radio Science Center for Space and Atmosphere, Kyoto University, Kyoto, Japan

S.-R. Zhang²

Haystack Observatory, Massachusetts Institute of Technology, Westford, Massachusetts, USA

Received 19 July 2002; revised 20 November 2002; accepted 20 February 2003; published 26 June 2003.

[1] Using a comprehensive data set from optical and radio instruments, we investigate a midnight brightness wave that appeared in 630-nm airglow images over Japan on the night of 9 September 1999. This may be the first such observation of the brightness wave with an all-sky imager in the East-Asian longitudinal sector. The imager at Shigaraki (35.6°N, 136.1°E) tracked a north-northeastward propagation of the wave with an apparent velocity of 500 m s⁻¹ after midnight. Ionosonde observations at five stations in Japan showed that rapid descent of the F_2 layer propagated northward beyond 35°N with decreasing amplitude. Incoherent scatter observations with the MU radar at Shigaraki also revealed that the F_2 peak altitude decreased from 360 to 280 km during the event. During the F_2 layer descent the altitude profile of the electron density became sharp, enhancing the F_2 peak electron density. After the F_2 layer altitude reached 280 km, electron density in the F_2 layer rapidly decreased because of increased neutral density at low altitude. A Fabry-Perot interferometer (FPI) at Shigaraki observed northward neutral winds of 10–70 m s⁻¹ during the event. A model calculation demonstrates that the meridional winds estimated from the MU radar electron density profiles are fairly consistent with those observed with the FPI. From these results we conclude that the observed northward wind enhancements, probably caused by the midnight temperature maximum, pushed down the plasma in the F_2 layer to lower altitudes along the geomagnetic field to cause the 630-nm airglow intensity enhancement. *INDEX TERMS*: 2427 Ionosphere: Ionosphere/atmosphere interactions (0335); 2437 Ionosphere: Ionospheric dynamics; 0310 Atmospheric Composition and Structure: Airglow and aurora; 2443 Ionosphere: Midlatitude ionosphere; 2415 Ionosphere: Equatorial ionosphere; *KEYWORDS*: midnight temperature maximum, 630-nm airglow, radar

Citation: Otsuka, Y., T. Kadota, K. Shiokawa, T. Ogawa, S. Kawamura, S. Fukao, and S.-R. Zhang, Optical and radio measurements of a 630-nm airglow enhancement over Japan on 9 September 1999, *J. Geophys. Res.*, 108(A6), 1252, doi:10.1029/2002JA009594, 2003.

1. Introduction

[2] Enhancements in 630-nm airglow at around midnight were observed for the first time by *Greenspan* [1966] and *Nelson and Cogger* [1971] in the American longitudinal sector. The recent observations conducted at Arequipa, Peru, and Arecibo, Puerto Rico, using all-sky CCD imagers revealed that the airglow enhancements propagated across the all-sky field of view [*Colerico et al.*, 1996; *Mendillo et al.*, 1997a]. These phenomena are called brightness waves by *Colerico et al.* [1996]. They showed seasonal occurrence of

the brightness waves over Arequipa. They used a Fabry-Perot interferometer (FPI) and a digital ionosonde to show enhancements in thermospheric temperature, poleward reversals of meridional neutral winds, and local minima in the zonal neutral winds during passage of the brightness waves. Radar studies by *Behnke and Harper* [1973] and *Harper* [1973] also revealed reversing winds from equatorward to poleward and sudden descents of the F_2 layer followed by a rapid decrease of the electron density, the so-called midnight collapse or midnight descent. The poleward winds shift the F_2 region plasma downward to the region of heavy chemical loss to produce enhancements in the oxygen 630-nm airglow emission [*Herrero and Meriwether*, 1980].

[3] The enhancement of poleward thermospheric wind is driven by a pressure bulge in the equatorial thermosphere. The bulge is induced by a local maximum in the diurnal variation of thermospheric temperature at around midnight

¹Now at Nihon Unisys, Ltd., Tokyo, Japan.

²On leave from Wuhan Institute of Physics and Mathematics, Chinese Academy of Sciences, Wuhan, China.

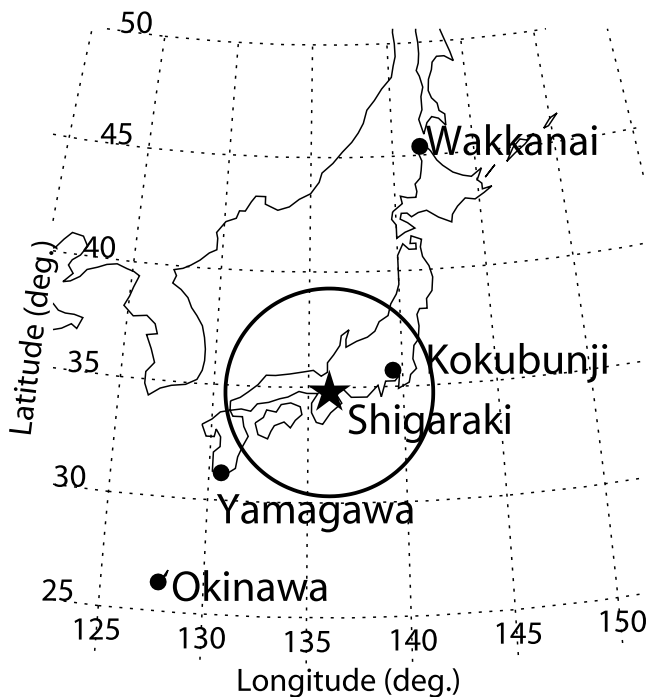


Figure 1. Locations of observation sites in geographic coordinates. The star represents the MU radar at Shigaraki, where the all-sky imager, FPI, and ionosonde are also located. Solid circles show other ionosonde stations. The field of view of the all-sky imager (60° off-zenith) is illustrated by the large, open circle, assuming an emission altitude of 250 km.

at low latitudes, the so-called Midnight Temperature Maximum (MTM). *Herrero and Spencer* [1982] analyzed the thermospheric temperature data from the AE-E satellite in 1971. They created temperature maps between $\pm 20^\circ$ geographic latitudes for each season to display the seasonal variation of MTM. Theoretical work on MTM was conducted by *Mayr et al.* [1979], *Herrero et al.* [1983], and *Fesen et al.* [1986]. They reported that MTM results from the interaction among atmospheric tides. *Fesen* [1996] used the Thermosphere/Ionosphere/Electrodynamical General Circulation Model (TIEGCM) of the National Center for Atmospheric Research and suggested that the seasonal variation of MTM may be caused by the interaction of the upward propagating semidiurnal tides with different modes.

[4] In this paper, using a comprehensive data set from multiple instruments, we report a brightness wave in 630-nm airglow over Japan and its related ionospheric phenomena on the night of 9 September 1999. This may be the first such observation of the brightness wave with an all-sky imager in the East-Asian longitudinal sector. We also use data taken from an FPI, the middle and upper atmosphere (MU) radar, and five ionosondes. Model calculations are conducted for the first time to investigate the observed phenomena quantitatively.

2. Observations

[5] The locations of the observation sites are displayed in Figure 1. The star shows the location of the MU radar,

Shigaraki (34.9°N , 136.1°E ; magnetic latitude (M-Lat): 25.6°), where an ionosonde is also operated. Four solid circles represent the locations of other ionosondes: Wakkanai (45.4°N , 141.7°E , M-Lat: 36.5°N), Kokubunji (35.7°N , 139.5°E , M-Lat: 26.5°N), Yamagawa (31.2°N , 130.6°E , M-Lat: 21.4°N), and Okinawa (26.3°N , 127.8°E , M-Lat: 16.3°N). At Shigaraki, an all-sky imager and a Fabry-Perot Interferometer (FPI) have been installed as parts of the Optical Mesosphere Thermosphere Imagers (OMTI) since 1998 [*Shiokawa et al.*, 1999]. The field of view of the imager observing 630-nm airglow is also shown in the figure. Two-dimensional patterns of 630-nm airglow are taken with a time resolution of 5.5 min. The FPI system and data processing schemes for calculating neutral wind velocity have been described by *Shiokawa et al.* [2001]. The FPI measures the fringe image of 630-nm airglow produced by optical interference with an etalon. The fringe image is divided into 16 azimuthal sectors. For each sector, line-of-sight wind velocity is calculated from the Doppler shift of the peak location of the fringe. Horizontal neutral wind velocity is derived with a time resolution of 20 min from 16 line-of-sight velocities with the Velocity-Azimuth Display (VAD) method, assuming that the wind velocity has no vertical component.

[6] The MU radar at Shigaraki [*Fukao et al.*, 1985a, 1985b] was operated in an incoherent scatter mode. The received power profile was normalized by using the F_2 peak density, $N_m F_2$, obtained from the Shigaraki ionosonde to produce the electron density profile at an altitude of 200 to 600 km. This $N_m F_2$ obtained from the ionosonde is also used in this study.

3. Results

3.1. All-Sky Airglow Observations

[7] Figure 2a shows a 2-hour sequence of the 630-nm airglow all-sky images measured at Shigaraki on the night of 9 September 1999. The center of each image corresponds to the location of Shigaraki. We can see a strong enhancement of the 630-nm intensity similar to brightness wave events reported by *Colerico et al.* [1996] and *Mendillo et al.* [1997a]. The 630-nm intensity starts to increase at the southwestern edge at 0248 LT, reaches a maximum at 0318 LT, and then decreases. The magnetic activity on 9–10 September 1999 was moderately quiet ($K_p = 1 \sim 4$).

[8] To show the motion of the 630-nm airglow enhancement, Figures 2b and 2c displays temporal variations of the 630-nm intensity between 2300 and 0500 LT along the north-south (latitudinal) and west-east (longitudinal) directions over Shigaraki. Using the method described by *Shiokawa et al.* [2000], the emission intensity is converted to absolute intensity in units of Rayleighs (R). The center of the vertical axis in each figure corresponds to the location of Shigaraki. The airglow intensity at the zenith reaches 130 R at around 0310 LT. The straight lines in Figures 2b and 2c represent the best fits to the intensity peaks. The apparent velocity of the airglow enhancement, which is derived from the slope of the lines, is 540 m s^{-1} toward the north and 1380 m s^{-1} toward the east. From the two apparent velocity components, it is found that the airglow enhancement propagates at 500 m s^{-1} in the

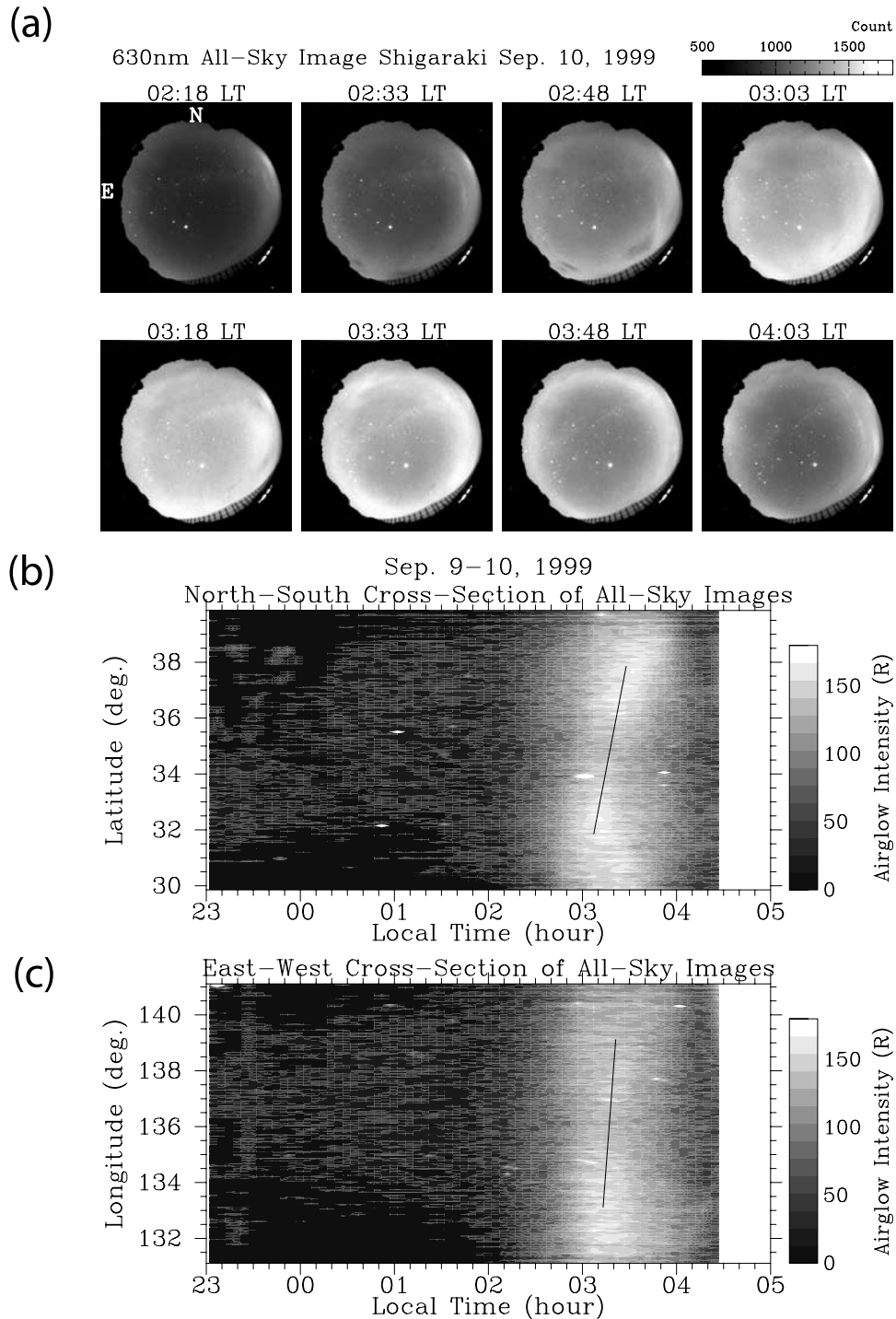


Figure 2. (a) Time sequence of the all-sky image at 630 nm measured at Shigaraki on the night of 9 September 1999. North is upward, and east is to the left. (b and c) Temporal variations of 630-nm airglow intensity in units of Rayleighs along north-south and west-east lines crossing the location of Shigaraki between 2300 and 0500 LT. The airglow emission layer is assumed to exist at an altitude of 250 km. The solid line in each figure connects points of peak airglow intensity. To obtain each solid line, a linear fit to the peak airglow intensity pattern was performed between $\pm 3^\circ$ in latitude (Figure 2b) and longitude (Figure 2c) centered at the location of Shigaraki. See color version of this figure at back of this issue.

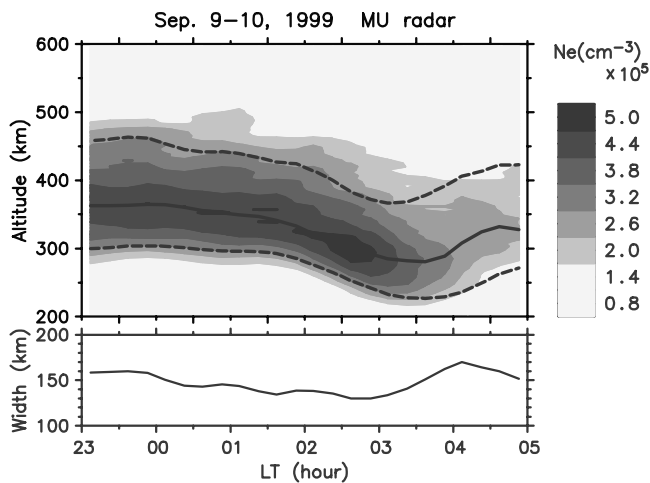


Figure 3. (top panel) Altitude-time contour of ionospheric electron density observed with the MU radar between 2300 and 0500 LT on the night of 9 September 1999. The solid curve shows the F_2 peak altitude. Dashed curves show altitudes where the electron density is reduced to 60% of the F_2 peak density at both the topside and bottomside of the F_2 layer. (bottom panel) Temporal variation of the F_2 layer width defined as a distance between the two dashed curves in the top panel. See color version of this figure at back of this issue.

north-northeast direction with an azimuth of 20° from the north.

3.2. MU Radar Incoherent Scatter Observations

[9] MU radar incoherent scatter observations provide electron density profiles over Shigaraki at an interval of 15 min. The altitude-time contour of the electron density between 2300 LT on 9 September 1999 and 0500 LT on the subsequent day is shown in the upper panel of Figure 3. Since the incoherent scatter echoes were weak, they suffered from large statistical fluctuations. To reduce these fluctuations, the electron density profiles were averaged with a moving window of 23 km in altitude and 45 min in time. The solid curve represents the F_2 peak altitude, and the two dashed curves represent the altitudes where the electron density is 60% of the F_2 peak density. The peak and topside altitudes of the F_2 layer start to descend at about 0000 LT, and the rate of descent become large after 0200 LT. The bottomside of the F_2 layer is rather stationary between 2300 and 0130 LT, and it descends after 0130 LT. The peak altitude reaches a minimum of 280 km at 0330 LT. Neutral particle density increases exponentially with decreasing altitude. Therefore when the F_2 layer moves downward, recombination of ions is accelerated and hence airglow intensity increases. This process is responsible for the airglow intensity enhancement between 0200 and 0400 LT (Figure 2). Following the descent of the F_2 layer, the electron density at lower altitudes decreases, largely because of rapid chemical loss.

[10] The F_2 layer descent occurred over the altitudes that included the topside and bottomside F_2 layer. The rate of descent depends on altitude. The F_2 layer descends more rapidly at higher altitude, which makes the altitude profile of the F_2 layer sharp and accumulates the F_2 layer plasma at

around the F_2 peak altitude. The lower panel of Figure 3 shows the temporal variation of the F_2 layer width, which is defined as the altitude difference between the two dashed curves in the upper panel. The width decreases from 160 km at 2300 LT to 130 km at 0245 LT. The sharpening of the F_2 layer contributes to the enhancement of the F_2 peak density at around 0200 LT.

3.3. Ionosonde Network Observations

[11] To investigate the spatial structure and extent of the F_2 layer descent and electron density decrease observed with the MU radar, the virtual height ($h'F$) of 3 MHz and F_2 peak density (N_mF_2) obtained every 15 min at five ionosonde stations are shown in Figure 4. The virtual height starts to descend rapidly in the order of Okinawa (0045 LT), Yamagawa (0100 LT), Shigaraki (0130 LT), and Kokubunji (0145 LT). The descent is larger at lower latitudes. On the other hand, the virtual height at Wakkanai descends gradually between 2315 and 0330 LT. These results indicate that the F_2 layer descent propagates from south to north with decreasing amplitude and subsides between Kokubunji (36°N) and Wakkanai (45°N).

[12] N_mF_2 observed at Okinawa, Yamagawa, Shigaraki, and Kokubunji starts to decrease at 0245–0315 LT. The N_mF_2 decrease is caused by the F_2 layer descent to lower altitudes, where the recombination rate of the plasma is larger. The amount of the N_mF_2 decrease is larger at lower latitudes. It is noteworthy that N_mF_2 slightly increases at around 0230–0300 LT, just before the rapid decrease. A similar increase of the F_2 peak density was observed with

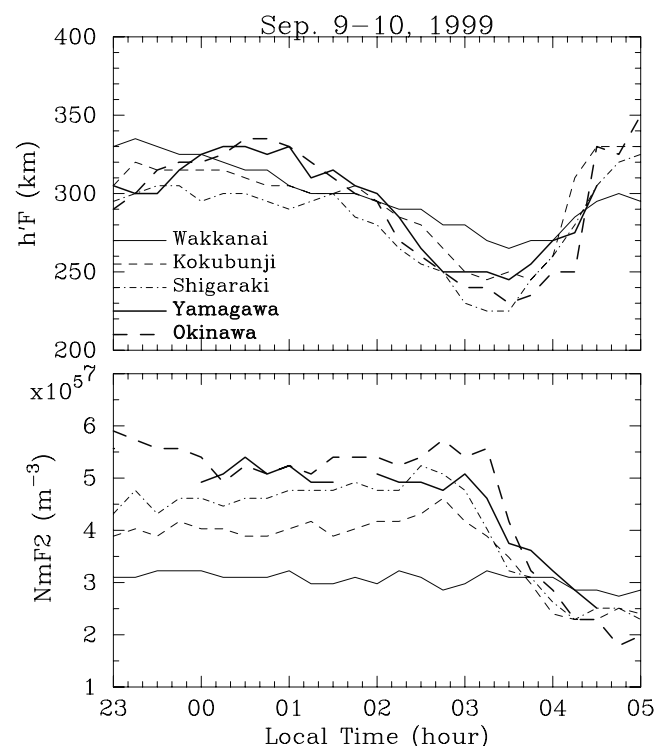


Figure 4. Temporal variations of F_2 peak density (N_mF_2) and virtual height ($h'F$) of 3 MHz observed with the ionosonde network in Japan between 2300 and 0500 LT on the night of 9 September 1999.

the MU radar (Figure 3). $N_m F_2$ at Wakkanai is almost stationary during the whole night.

3.4. Fabry-Perot Interferometer Observations

[13] Figure 5 shows temporal variations in the southward neutral wind velocity observed with the Fabry-Perot interferometer (FPI) at Shigaraki on the night of 9 September 1999. Error bars represent the possible errors of neutral wind velocity estimation, which is determined as residuals of the sinusoidal fitting procedure with the Velocity-Azimuth Display (VAD) method. The accuracy is worse until 0100 LT because the sky was slightly cloudy in the northern parts of the images. The dashed curve shows the mean neutral wind velocity in the autumn (9 August to 6 November) of 1999 [Shiokawa *et al.*, 2003]. This mean wind velocity shows an equatorward peak at around the postmidnight hours, becomes gradually weaker with time, and changes to the poleward direction before 0300 LT. On the night of 9 September, however, wind direction reversed at about 0130 LT and the poleward wind reached 70 m s^{-1} at 0330 LT. The difference between the mean and observed winds is $40\text{--}70 \text{ m s}^{-1}$ for 0130–0400 LT. This poleward enhancement of the neutral wind probably caused the descent of the F_2 layer along the geomagnetic field to lower altitudes, as shown in Figure 3.

[14] Figure 6 shows temporal variations in the neutral temperature observed with the Fabry-Perot interferometer (FPI) at Shigaraki on the night of 9 September 1999. The neutral temperature increased from 700 to 1000 K and reached a maximum at 0250 LT. The temperature enhancement is called Midnight Temperature Maximum (MTM). Colerico *et al.* [1996] and Mendillo *et al.* [1997a] have defined the midnight brightness wave as a poleward propagating 630-nm airglow enhancement specifically correlated

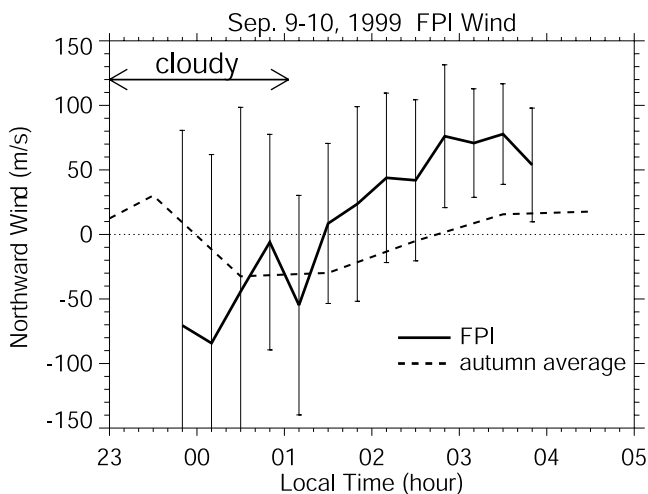


Figure 5. Temporal variation of meridional neutral wind velocity (positive northward) observed with a Fabry-Perot interferometer at Shigaraki between 2300 and 0500 LT on the night of 9 September 1999. An error bar indicates the estimation error of neutral wind velocity, which is determined as residuals of the sinusoidal fitting procedure with the Velocity-Azimuth Display (VAD) method. The dashed line shows the mean neutral wind velocity in autumn, which is obtained by averaging neutral wind data during the period from 9 August to 6 November 1999.

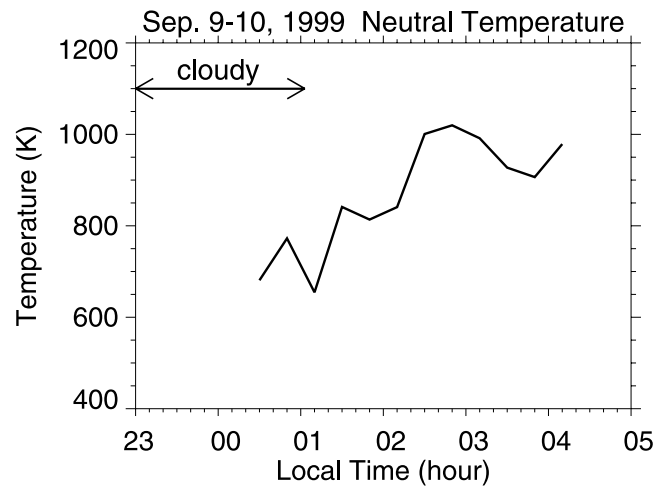


Figure 6. Temporal variation of neutral temperature observed with a Fabry-Perot interferometer at Shigaraki between 2300 and 0500 LT on the night of 9 September 1999.

with increases in neutral temperature. Therefore the 630-nm airglow enhancement observed at Shigaraki (Figure 2) is regarded as a midnight brightness wave.

4. Comparison With Model Calculations

4.1. Airglow Intensity

[15] As shown above, strong enhancement of 630-nm airglow intensity was observed over Shigaraki. The MU radar simultaneously observed the decrease of the F_2 layer altitude by 80 km, resulting in an increase in the electron density at the 630-nm emission altitude of around 250 km. To examine whether this downward motion of the F_2 layer to lower altitudes where molecular oxygen is rich is sufficient to produce the observed 630-nm enhancement ($\sim 110 \text{ R}$), we conducted a model calculation using the electron density profiles obtained from the MU radar. Neutral density and temperature are taken from the Mass Spectrometer and Incoherent Scatter (MSIS) model [Hedin, 1987]. Briefly, the 630-nm emission results from dissociative recombination of O_2^+ , which is produced by charge exchange between O^+ and O_2 ($\text{O}^+ + \text{O}_2 \rightarrow \text{O} + \text{O}_2^+$; $\text{O}_2^+ + e^- \rightarrow \text{O} + \text{O} + h\nu(630\text{nm})$). Since the dissociative recombination is rapid, the 630-nm volume emission rate is controlled by the charge exchange reaction, and is thus proportional to the product of the O^+ and O_2 densities. To calculate the volume emission rate, we adopted an equation given by Sobral *et al.* [1993]. Ogawa *et al.* [2002] have also used this method to quantitatively compare variations in the 630-nm airglow and total electron content produced by traveling ionospheric disturbances.

[16] Figure 7 shows a contour plot of the calculated volume emission rate of 630-nm airglow as a function of altitude and time on the night of 9 September 1999. The solid curve shows the altitude of the peak volume emission rate. During 0030–0130 LT the peak altitude is around 290 km and the airglow layer expands between 250 and 350 km altitudes. The peak altitude decreases gradually after 0130 LT and reaches a minimum of 240 km at 0320 LT. The F_2 peak altitude is also shown by the dashed curve in the figure. From comparison between two curves, the altitude

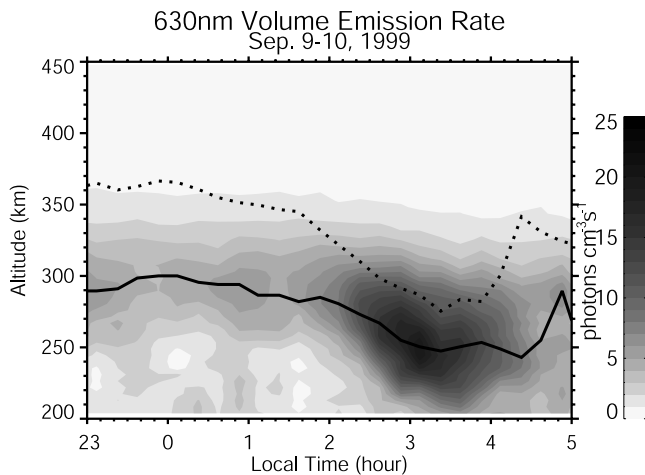


Figure 7. Time-altitude cross section of the volume emission rate of 630-nm airglow. The volume emission rate is calculated from electron density measured with the MU radar and neutral density taken from the MSIS model. The solid curve shows the altitude of the peak volume emission rate. The dashed curve shows the F_2 peak altitude.

variation of the emission layer is found to follow that of the F_2 layer with offsets of 50–70 km between the peak altitudes of the F_2 layer and the emission layer. The F_2 peak altitude decreased by 80 km during the night. This altitude variation was more than twice the scale height of molecular oxygen, O_2 , which is approximately 30 km. Since the O^+ density is nearly equal to the electron density in the F region and the airglow emission rate is proportional to the product of the O_2 and O^+ densities, the volume emission rate increases about seven times ($e^2 = 7.4$) as the F_2 layer descends by two scale heights.

[17] Integrating the volume emission rate over altitude gives the total emission intensity to be observed on the ground. Figure 8 displays a comparison between the calculated total emission and the observed airglow intensity at the zenith of Shigaraki. The general features of the temporal variation of the observed airglow intensity are well reproduced in the model calculation, although the modeled intensity is 0–30 R higher than the observed one during the whole observation period. Both the observed and modeled airglow intensities start to increase at 0140 LT, reach their maxima around 0310 LT, and decrease until sunrise. Agreement between the temporal variations of the observed and modeled airglow intensity implies that the airglow enhancement of 110 R observed with the all-sky imager is caused by the electron density variation at the bottomside of the F_2 layer which results from the descent of the F_2 layer by 80 km.

[18] The offset of 0–30 R might be due to calibration uncertainty of the all-sky imager. Absorption of the airglow due to O_3 , CO_2 , H_2O , and so on also contributes to decreasing the observed airglow intensity. Here, we assume that the offset is constant and equal to 30 R. This value is determined to adjust the modeled intensity to the observed intensity during the period of 0000–0130 LT when both intensities are almost stationary. The thin curve in Figure 8 represents modified intensity obtained by subtracting the constant intensity (30 R) from the modeled intensity. The modified intensity agrees fairly well with the observed

intensity until the modified intensity reaches the peak at 0300 LT, and subsequently, the observed intensity becomes larger than the modified intensity. It is noted that the discrepancy between the observed and modified intensities starts when electron density rapidly decreases (Figure 3).

[19] This can be related to the red line hysteresis effect. *Cogger et al.* [1980] explained this effect as follows. After the descent of the F_2 layer, the electron density is rapidly reduced, especially at the bottomside of the F_2 layer because of high neutral density. The lifetime of O_2^+ becomes long in a region where electron density is low, and the ion density distribution is influenced by transport due to ambipolar diffusion. O_2^+ , which is produced by charge exchange between O^+ and O_2 , diffuses to the region of lower O_2^+ density. They are not in chemical equilibrium. Therefore the model calculation used in this paper, in which the chemical equilibrium is assumed, may underestimate the airglow intensity.

4.2. Meridional Neutral Winds

[20] Meridional neutral wind velocity is computed by using a one-dimensional numerical model developed by *Zhang and Huang* [1995] and *Zhang et al.* [1999]. The model solves the O^+ diffusion equation derived from corresponding continuity and momentum equations. It takes account of the main photochemical processes for O^+ , NO^+ , O_2^+ and N_2^+ between 100 and 500 km of altitude. The neutral density and temperature are given by MSIS86 [*Hedin*, 1987] and solar fluxes by the EUVAC model [*Richards et al.*, 1994]. Plasma temperatures are given by average values obtained from MU radar measurements [*Otsuka et al.*, 1998]. F_2 peak altitudes observed with the MU radar (shown in Figure 3) are used as input to the model calculation to obtain the meridional neutral wind velocity average over 220–450 km. Electric fields are not included in this calculation.

[21] Figure 9 shows a comparison between the northward neutral winds obtained from the FPI observations (Figure 5)

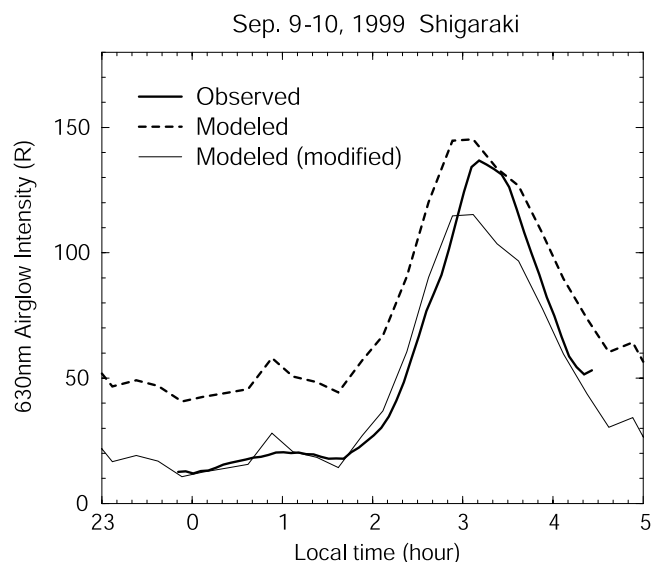


Figure 8. Comparison of 630-nm airglow intensity between (thick curve) observation of the all-sky imager and (dashed curve) the model calculation. The thin curve shows modified intensity, which is obtained by subtracting 30 R from the modeled intensity.

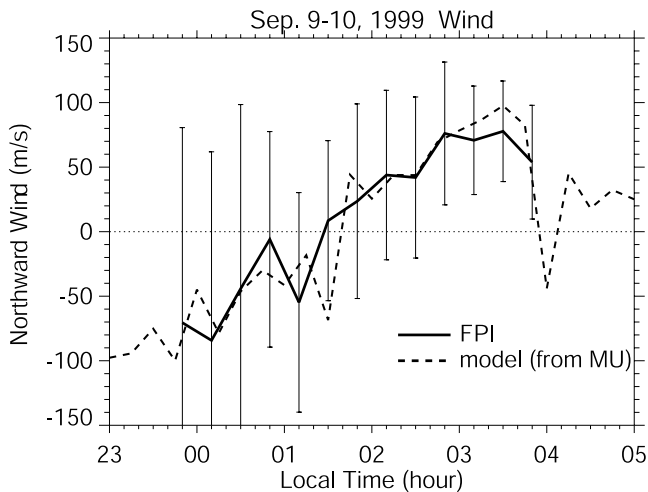


Figure 9. Comparison between (solid line) observed and (dashed line) modeled neutral wind velocities (positive northward). The solid line and error bars are same as those in Figure 5. The dashed line shows the modeled wind calculated using the electron density profiles obtained from the MU radar on the night of 9 September 1999 (Figure 3).

and the model calculation. The measured wind is reproduced well by the model calculation. This result indicates that the height variations of the F_2 layer are caused by the poleward neutral winds and that effect of electric fields is negligible.

5. Discussion

[22] The midnight brightness wave is caused by poleward winds generated by the midnight temperature maximum (MTM) at low latitudes [Herrero and Meriwether, 1980; Colerico *et al.*, 1996; Mendillo *et al.*, 1997a, 1997b]. Colerico *et al.* [1996] analyzed all-sky images of 630-nm airglow obtained at Arequipa, Peru (16.2°S , 71.4°W) during two periods, 8–22 October 1993 and 23 September to 9 October 1994.

[23] They reported that the propagation direction of pre-midnight and midnight brightness waves showed significant local time dependence: equatorward and poleward, respectively. The average apparent meridional velocity of the pre-midnight brightness wave was $356 \pm 179 \text{ m s}^{-1}$ and $248 \pm 31 \text{ m s}^{-1}$ (October 1993) and $368 \pm 70 \text{ m s}^{-1}$ (October 1994) for the midnight brightness wave.

[24] Mendillo *et al.* [1997b] reported similar features of brightness waves over Arecibo, Puerto Rico (18.3°N , 66.75°W). The brightness wave that we observed at Shigaraki appeared at 0200–0400 LT and propagated poleward (azimuth of 20° from the north) with an apparent meridional velocity of 540 m s^{-1} . These propagation characteristics are consistent with those at the American longitudinal sector, although the apparent meridional velocity is slightly larger.

[25] While AE-E satellite observations [Spencer *et al.*, 1979] and TIEGCM calculations [Fesen, 1996] show that the longitudinal variation of MTM is not discernible, our result suggests possibility of the longitudinal variation existing. Colerico and Mendillo [2002] have suggested possible longitude dependencies in the MTM characteristics

by comparing ground based observations of the MTM in the American sector and the Indian sector.

[26] The all-sky imager at Shigaraki has been operated since October 1998. We analyzed two-dimensional patterns on 630-nm airglow intensity images obtained from October 1998 to December 2000 and found three events of brightness waves that propagated poleward across the all-sky field of view. Thus these events seem to be rare over Japan. At Arecibo, Mendillo *et al.* [1997b] have conducted all-sky imager observations during 19–28 January 1993 and 21 February to 22 August 1995. In these 6-month campaign periods, these potential brightness waves were observed on four nights. The higher occurrence rate of brightness waves at Arecibo is probably due to its low geographic latitude (18°N). The result presented in this paper shows that winds probably generated from the MTM pressure bulge may propagate up to 40°N in the Japanese sector.

[27] Generally, neutral winds in the nighttime thermosphere flow equatorward because of the pressure gradient force caused by solar EUV heating of the daytime thermosphere. The equatorward wind pushes up the plasma in the F_2 layer along the geomagnetic field. Altitudes of the F_2 layer are determined from the balance between upward motion due to the equatorward winds and downward motion due to gravitationally induced ion diffusion. Although the electric field also contributes upward or downward motions of the plasma, this effect is relatively small at midlatitudes [e.g., Balan *et al.*, 1998]. If the equatorward wind is weakened, it lowers the F_2 layer to a new balanced height. At the lower altitudes, the ion collision frequency increases to decrease the gravity diffusion. However, when the neutral wind is reversed to poleward, nothing is balanced with the diffusion, which is always downward, resulting in significant downwelling of the F_2 layer. The gravity diffusion velocity increases with altitude because of the decrease in the neutral density. This is the reason that the F_2 layer above its peak altitude descends more rapidly than the bottomside of the F_2 layer on the night of 9 September 1999 (upper panel of Figure 3). The altitude-dependent downward velocity decreases the F_2 layer width (lower panel of Figure 3). The F_2 layer plasma is accumulated around the F_2 peak altitude, and thus the F_2 peak density is enhanced around 0240 LT. The enhancement of the F_2 peak density before the rapid descent of the F_2 layer was also observed with four ionosondes at Okinawa, Yamagawa, Shigaraki, and Kokubunji (Figure 4).

[28] Shiokawa *et al.* [2002] also have observed similar variations in N_mF_2 , F_2 layer height, and 630-nm airglow during the passage of a large-scale traveling ionospheric disturbance propagating equatorward during a magnetic storm. They compared the observations with the Sheffield University Plasmasphere Ionosphere Model [e.g., Bailey *et al.*, 1997], and concluded that the observed features of N_mF_2 , F_2 layer height and 630-nm airglow were caused by an enhancement of poleward neutral wind. These observations suggest that the northward wind enhancement produces the F_2 peak electron density enhancement before the descent of the F_2 layer.

6. Conclusions

[29] We observed a midnight brightness wave related to the midnight temperature maximum with an all-sky imager

at Shigaraki, Japan. This may be the first such observation in the East-Asian longitudinal sector. The 630-nm airglow enhancement propagated toward the north-northeast (azimuth of 20° from the north) with an apparent velocity of 500 m s^{-1} . The propagation direction of the airglow enhancement is consistent with brightness waves observed in the American longitudinal sector, although the apparent meridional velocity is slightly larger.

[30] Incoherent scatter observations with the MU radar revealed that the F_2 peak altitude decreased from 360 to 280 km between 0100 and 0330 LT. The F_2 layer descent was more rapid at higher altitudes, making the altitude profile of the F_2 layer sharp enhancing the F_2 peak electron density. After the F_2 peak altitude reached 280 km, the electron density in the F_2 layer rapidly decreased because of increased neutral density at lower altitudes.

[31] Ionosonde observations at five locations showed that the brightness wave and its related phenomena moved from south to north with decreasing amplitude and subsided somewhere between Kokubunji (36°N) and Wakkanai (45°N). An FPI at Shigaraki observed northward neutral winds of $10\text{--}70 \text{ m s}^{-1}$ at 0110–0400 LT. Model calculations confirmed quantitatively that the northward winds pushed down the F_2 layer along the geomagnetic field to lower altitudes, causing enhancement of the 630-nm airglow intensity.

[32] **Acknowledgments.** We thank Y. Katoh, M. Satoh, and T. Katoh of the Solar-Terrestrial Environment Laboratory, Nagoya University, for their kind support of airglow imaging observations. The MU radar is owned and operated by the Radio Science Center for Space and Atmosphere of Kyoto University. Ionograms were provided through the World Data Center for Ionosphere of the Communications Research Laboratory, Tokyo. This work was supported by a Grant-in-Aid for Scientific Research of the Ministry of Education, Culture, Sports, Science and Technology of Japan (11440145).

[33] Arthur Richmond thanks M. Colerico and Jose Humberto A. Sobral for their assistance in evaluating this paper.

References

- Bailey, G. J., N. Balan, and Y. Z. Su, The Sheffield University plasmasphere ionosphere model—a review, *J. Atmos. Terr. Phys.*, **59**, 1541–1552, 1997.
- Balan, N., Y. Otsuka, G. J. Bailey, and S. Fukao, Equinoctial asymmetries in the ionosphere and thermosphere observed by the MU radar, *J. Geophys. Res.*, **103**, 9481–9495, 1998.
- Behne, R. A., and R. M. Harper, Vector measurements of F region ion transport at Arecibo, *J. Geophys. Res.*, **78**, 8222–8233, 1973.
- Cogger, L. L., J. C. G. Walker, J. W. Meriwether Jr., and R. G. Burnside, F region airglow: Are ground-based observations consistent with recent satellite results?, *J. Geophys. Res.*, **85**, 3013–3020, 1980.
- Colerico, M., and M. Mendillo, The current state of investigations regarding the thermospheric midnight temperature maximum (MTM), *J. Atmos. Sol. Terr. Phys.*, **64**, 1361–1369, 2002.
- Colerico, M., M. Mendillo, D. Nottingham, J. Baumgardner, J. Meriwether, J. Mirick, B. W. Reinisch, J. L. Scali, C. G. Fesen, and M. A. Biondi, Coordinated measurements of F region dynamic related to the thermospheric midnight temperature maximum, *J. Geophys. Res.*, **101**, 26,783–26,793, 1996.
- Fesen, C. G., Simulations of the low-latitude midnight temperature maximum, *J. Geophys. Res.*, **101**, 26,863–26,873, 1996.
- Fesen, C. G., R. E. Dickinson, and R. G. Roble, Simulation of the thermospheric tides at equinox with the National Center for Atmospheric Research Thermospheric General Circulation Model, *J. Geophys. Res.*, **91**, 4471–4489, 1986.
- Fukao, S., T. Sato, T. Tsuda, S. Kato, K. Wakasugi, and T. Makihiro, The MU radar with an active phased array system: 1. Antenna and power amplifiers, *Radio Sci.*, **20**, 1155–1168, 1985a.
- Fukao, S., T. Tsuda, T. Sato, S. Kato, K. Wakasugi, and T. Makihiro, The MU radar with an active phased array system: 2. Inhouse equipment, *Radio Sci.*, **20**, 1169–1176, 1985b.
- Greenspan, J. A., Synoptic description of the 6300 Å nightglow near 78° west longitude, *J. Atmos. Terr. Phys.*, **28**, 739–745, 1966.
- Harper, R. M., Nighttime meridional neutral winds near 350 km at low to mid-latitudes, *J. Atmos. Terr. Phys.*, **35**, 2023–2034, 1973.
- Hedin, A. E., MSIS-86 thermospheric model, *J. Geophys. Res.*, **92**, 4642–4649, 1987.
- Herrero, F. A., and J. W. Meriwether, 6300 Å airglow meridional intensity gradients, *J. Geophys. Res.*, **85**, 4194–4204, 1980.
- Herrero, F. A., and N. W. Spencer, On the horizontal distribution of the equatorial thermospheric midnight temperature maximum and its seasonal variation, *Geophys. Res. Lett.*, **9**, 1179–1182, 1982.
- Herrero, F. A., H. G. Mayr, and N. W. Spencer, Latitudinal (seasonal) variation in the thermospheric midnight temperature maximum: A tidal analysis, *J. Geophys. Res.*, **88**, 7225–7235, 1983.
- Mayr, H. G., I. Harris, N. W. Spencer, A. E. Hedin, L. E. Wharton, H. S. Porter, J. C. G. Walker, and H. C. Carlson Jr., Tides and the midnight temperature anomaly in the thermosphere, *Geophys. Res. Lett.*, **6**, 447–450, 1979.
- Mendillo, M., J. Baumgardner, M. Colerico, and D. Nottingham, Imaging science contributions to equatorial aeronomy: Initial results from the MISETA program, *J. Atmos. Terr. Phys.*, **59**, 1587–1599, 1997a.
- Mendillo, M., J. Baumgardner, D. Nottingham, J. Aarons, B. Reinisch, J. Scali, and M. Kelley, Investigations of thermospheric-ionospheric dynamics with 6300 Å images from the Arecibo observatory, *J. Geophys. Res.*, **102**, 7331–7343, 1997b.
- Nelson, G. J., and L. L. Cogger, Dynamical behavior of the nighttime ionosphere at Arecibo, *J. Atmos. Terr. Phys.*, **33**, 1711–1726, 1971.
- Ogawa, T., N. Balan, Y. Otsuka, K. Shiokawa, C. Ihara, T. Shimomai, and A. Saito, Observations and modeling of 630 nm airglow and total electron content associated with traveling ionospheric disturbances over Shigaraki, Japan, *Earth Planets Space*, **54**, 45–56, 2002.
- Otsuka, Y., S. Kawamura, N. Balan, S. Fukao, and G. J. Bailey, Plasma temperature variations in the ionosphere over the middle and upper atmosphere radar, *J. Geophys. Res.*, **103**, 20,705–20,713, 1998.
- Richards, P. G., J. A. Fennelly, and D. G. Torr, EUVAC: A solar EUV flux model for aeronomic calculations, *J. Geophys. Res.*, **99**, 8981–8992, 1994.
- Shiokawa, K., Y. Katoh, M. Satoh, M. K. Ejiri, T. Ogawa, T. Nakamura, T. Tsuda, and R. H. Wiens, Development of optical mesosphere thermosphere imagers (OMTI), *Earth Planets Space*, **51**, 887–896, 1999.
- Shiokawa, K., Y. Katoh, M. Satoh, M. K. Ejiri, and T. Ogawa, Integrating-sphere calibration of all-sky cameras for nightglow measurements, *Adv. Space Res.*, **26**, 1025–1028, 2000.
- Shiokawa, K., T. Kadota, M. K. Ejiri, Y. Otsuka, Y. Katoh, M. Satoh, and T. Ogawa, Three-channel imaging Fabry-Perot interferometer for measurement of mid-latitude airglow, *Appl. Opt.*, **40**, 4286–4296, 2001.
- Shiokawa, K., Y. Otsuka, T. Ogawa, N. Balan, K. Igarashi, A. J. Ridley, D. J. Knipp, A. Saito, and K. Yumoto, A large-scale traveling ionospheric disturbance during the magnetic storm of 15 September 1999, *J. Geophys. Res.*, **107**(A6), 1088, doi:10.1029/2001JA000245, 2002.
- Shiokawa, K., T. Kadota, Y. Otsuka, T. Ogawa, T. Nakamura, T. Tsuda, and S. Fukao, A two-channel Fabry-Perot interferometer with thermoelectric-cooled CCD detectors for neutral wind measurement in the upper atmosphere, *Earth Planets Space*, in press, 2003.
- Sobral, J. H. A., H. Takahashi, M. A. Abdu, P. Muralikrishna, Y. Sahai, C. J. Zamlutti, E. R. de Paula, and P. P. Batista, Determination of the quenching rate of the $\text{O}(\text{^1D})$ by $\text{O}(\text{^3D})$ from rocket-borne optical (630 nm) and electron density data, *J. Geophys. Res.*, **98**, 7791–7798, 1993.
- Spencer, N. W., G. R. Carignan, H. G. Mayr, H. B. Niemann, R. F. Theis, and L. E. Wharton, The midnight temperature maximum in the Earth's equatorial thermosphere, *Geophys. Res. Lett.*, **6**, 444–446, 1979.
- Zhang, S.-R., and X.-Y. Huang, A numerical study of ionospheric profiles for mid-latitudes, *Ann. Geophys.*, **13**, 551–557, 1995.
- Zhang, S.-R., S. Fukao, and W. L. Oliver, Data modeling and assimilation studies with the MU radar, *J. Atmos. Sol. Terr. Phys.*, **61**, 563–583, 1999.

S. Fukao and S. Kawamura, Radio Science Center for Space and Atmosphere, Kyoto University, Gokasho, Uji, 611-0011, Japan. (fukao@kurasc.kyoto-u.ac.jp; kawamura@kurasc.kyoto-u.ac.jp)

T. Kadota, Nihon Unisys, Ltd., 1-1-1 Toyosu, Koto-ku, 135-8560, Tokyo, Japan.

T. Ogawa, Y. Otsuka, and K. Shiokawa, Solar-Terrestrial Environment Laboratory, Nagoya University, 3-13 Honohara, Toyokawa, 442-8507 Aichi, Japan. (ogawa@stelab.nagoya-u.ac.jp; otsuka@stelab.nagoya-u.ac.jp; shiokawa@stelab.nagoya-u.ac.jp)

S.-R. Zhang, Haystack Observatory, Massachusetts Institute of Technology, Westford, MA 01886, USA. (shunrong@haystack.edu)

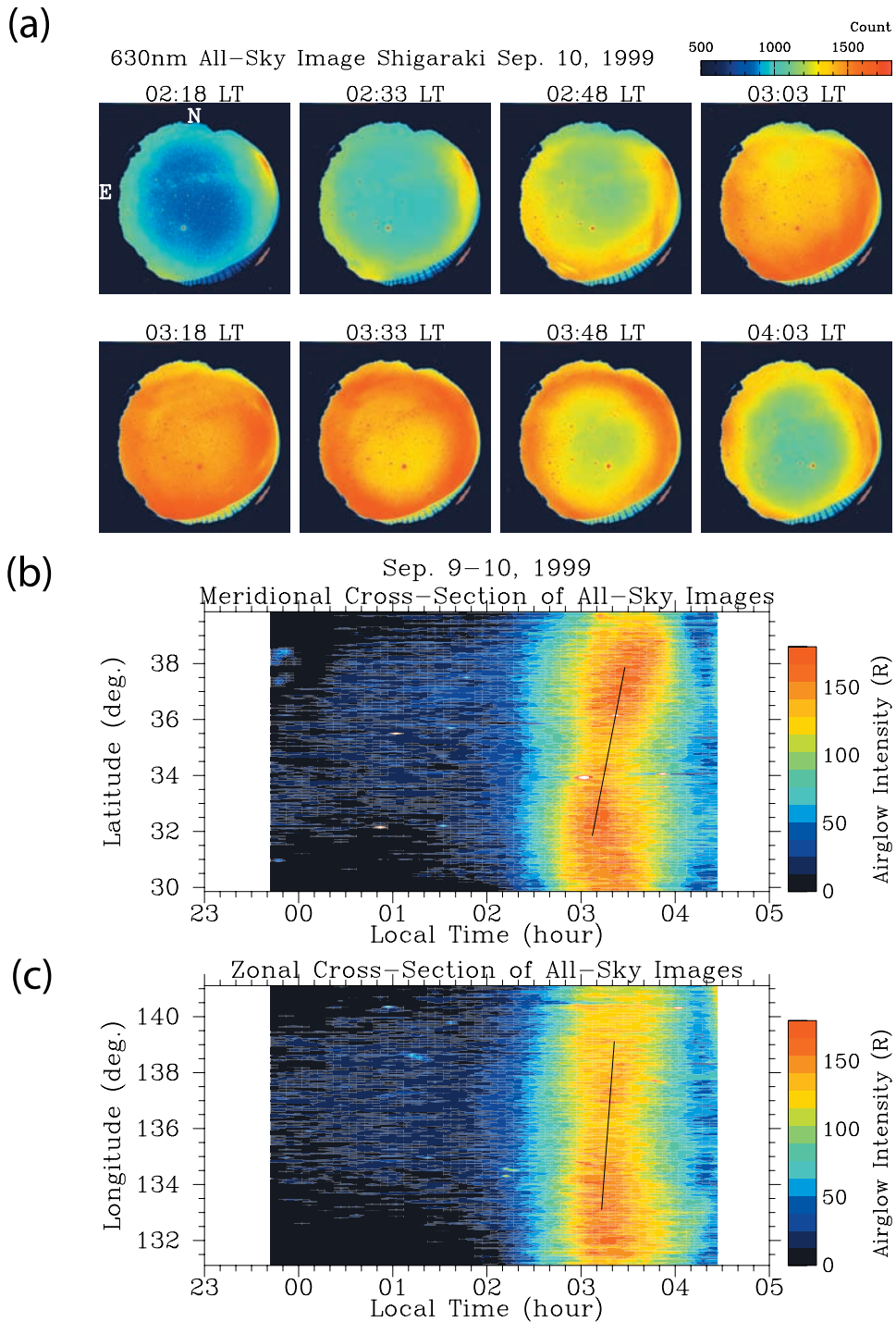


Figure 2. (a) Time sequence of the all-sky image at 630 nm measured at Shigaraki on the night of 9 September 1999. North is upward, and east is to the left. (b and c) Temporal variations of 630-nm airglow intensity in units of Rayleighs along north-south and west-east lines crossing the location of Shigaraki between 2300 and 0500 LT. The airglow emission layer is assumed to exist at an altitude of 250 km. The solid line in each figure connects points of peak airglow intensity. To obtain each solid line, a linear fit to the peak airglow intensity pattern was performed between $\pm 3^\circ$ in latitude (Figure 2b) and longitude (Figure 2c) centered at the location of Shigaraki.

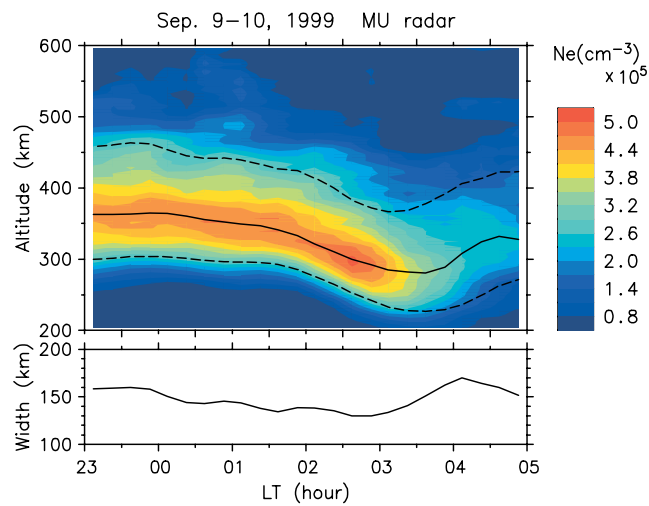


Figure 3. (top panel) Altitude-time contour of ionospheric electron density observed with the MU radar between 2300 and 0500 LT on the night of 9 September 1999. The solid curve shows the F_2 peak altitude. Dashed curves show altitudes where the electron density is reduced to 60% of the F_2 peak density at both the topside and bottomside of the F_2 layer. (bottom panel) Temporal variation of the F_2 layer width defined as a distance between the two dashed curves in the top panel.